Ocean Engineering 302 (2024) 117687

Contents lists available at ScienceDirect

Ocean Engineering

journal homepage: www.elsevier.com/locate/oceaneng

Research paper

Numerical analysis of performance of wavebreakers exposed to regular waves in static and floating configuration

Giacomo Rismondo [*,1], Vincenzo Armenio [1]

Dipartimento di Ingegneria e Architettura, Universitá degli Studi di Trieste, Piazzale Europa, 1, Trieste, 34127, Italy

ARTICLE INFO

Keywords:
Unsteady Reynolds Average Navier Stokes equations URANS
Fluid Structure Interaction FSI
Single Degree of Freedom SDOF
Wave generation and propagation

ABSTRACT

In the present paper we investigate, through numerical analysis, the hydrodynamic behavior of wavebreakers both in static and in floating configuration. The aim is to evaluate and compare the performance of wavebreakers in regular waves in the range of intermediate depth waters. The analysis is performed through evaluation of the waves transmitted downward and reflected back and the dissipative behavior of the wavebreaker. We simulate numerically the fluid dynamic field using the Unsteady Reynolds Averaged Navier Stokes equations (URANS) with the $k-\epsilon$ turbulence model, both for the water and the air phases, using the Volume of Fluid (VOF) method to detect the interface. We simulate a numerical wave tank, generating the waves at a lateral boundary of the domain and allowing its own propagation into the domain. First we study the static configuration of the wavebreaker, so it is considered fixed in space. Afterward, we consider the wavebreaker as a rigid body with a Single Degree of Freedom (SDOF) in the vertical direction and we analyze the interaction between the wave system and the structure. With this purpose we use the URANS equations over a dynamic mesh in conjunction with a Fluid–Structure-Interaction (FSI) algorithm, where the mesh displacement is associated to the body's motion through a diffusive Laplace equation; the motion of the solid body is evaluated using the momentum equation of a rigid body subject to hydrodynamic loading. We study two different wavebreakers, the rectangular one and the Π shape one, and evaluate the differences in terms of transmitted, reflected and dissipated energy.

First we assess the algorithm of generation and propagation of the regular waves comparing numerical results with analytical data. Afterward, we evaluate the performance of the two wavebreakers in terms of coefficients of transmission, reflection and dissipation and we compare our numerical results with data from the standard Wiegel Theory, 1960 and successive modifications. Finally, we study the performance of the wave system in presence of the floating body. This is done in two steps: we initially validate the results with those of the analytical solution of the governing equation of a SDOF rigid body forced by regular wave trains; successively we calculate the transmission coefficients for a number of waves with different length and height and compare the results with literature empirical formulas.

1. Introduction

The study of wavebreakers is an important field of research in maritime and coastal engineering. These devices are widely used for several applications; among others, they are used to protect harbors, marinas, offshore petroleum platforms, or other kinds of marine infrastructure from the action of waves and storms. The big impact of their use on the economy and industrial progress of a country gives these infrastructures a very important role (Sadeghi, 2008). They are also employed for the reduction of coastal erosion, which in recent years has particularly intensified due to anthropogenic activities (Van Rijn, 2011). Also, they may be used as Wave Energy Conversion (WEC) systems, devices that convert the energy of the waves into zero-emission electric energy. In particular, the integration of different types of clean energy devices (for example the WECs with floating wind turbines, platforms, and wavebreakers) is crucial to reduce the total Levelised Cost of Energy (LCoE) (Abhinav et al., 2020).

The operation principle of a wavebreaker consists of reflection of the incident wave and dissipation of a fraction of the wave energy through the formation of a swirling and dissipative fluid motion. As a result, the wave energy transmitted behind the body is a small portion of the energy of the incident wave. Here we focus on floating breakwaters (FB) which represent a subset of the general class of wavebreakers and

* Corresponding author.
E-mail addresses: giacomo.rismondo@phd.units.it (G. Rismondo), vincenzo.armenio@dia.units.it (V. Armenio).
[1] These authors contributed equally to this work.

https://doi.org/10.1016/j.oceaneng.2024.117687
Received 25 October 2023; Received in revised form 11 March 2024; Accepted 25 March 2024
Available online 30 March 2024

are used in several situations. They are placed in the free surface region where most of the wave energy is concentrated (Falcão, 2010) since more than 90% of the total energy of the wave is distributed within a depth three times the wave height below the free surface. Therefore, the floating wavebreakers represent an interesting alternative to their counterparts resting on the seabed, as their construction is not affected by the water depth and conditions of the seafloor. In addition, the tidal variations of the sea surface have a limited effect on floating structures. An additional advantage of these systems is that they do not inhibit the water circulation within the basin to be protected by the action of the sea waves. An important and challenging problem related to the use of FBs is their utilization as an energy dissipation system. Their efficiency is related to the incident wave conditions. As found in the previous studies of Gaythwaite (1987) and Cox and Beach (2006) the performance of FBs deteriorates for high wave or resonant periods and they are more effective when subject to short wave periods. Therefore is essential to investigate the FB performance under typical sea conditions and individuate the range of applications of these devices.

Despite these limitations, there are several practical applications where FB is successfully installed. Among the others, we mention the installation of Fazzano (Portovenere, Italy) composed of 22 modules of FBs with the dimension 20 × 4 m each, anchored with chains and deadweights (http://www.ingemar.it/en/672references&nos=1). In this particular case, they were found to be very effective, since the fetch in the area is such to produce short waves.

There are four general classes of FB: Pontoon; Box; Tethered Float; Mat Bruce (1985). Within the family of Box FB, the Π-shape is known to be very efficient; This geometrical configuration was initially studied by Gesraha (2006). Other new-generation FB were recently developed. Among them we mention the L-type one, analyzed through laboratory experiments by Neelamani and Rajendran (2002) and the F-type investigated numerically and experimentally by Wenyang et al. (2017). Further, a FB composed of two elongated cylinders and a mesh of suspending balls was studied by Chun-Yan et al. (2015) through an experimental analysis, whereas (Hong et al., 2015) analyzed the wave attenuation characteristics of a flexible FB.

The key parameter to be quantified in the analysis of wavebreakers is the transmission coefficient, defined as the ratio between the height of the wave transmitted behind the obstacle and that of the incident wave. Macagno (1954) developed a formula to assess the transmission coefficient for a rectangular, fixed and infinitely long wavebreaker with a draft d and subject to the action of regular waves. The use of this formula is restricted to the rectangular box-type wavebreaker, and has intrinsic limitations like the fact that if the draft is equal to the depth of the water column the transmission coefficient is not zero. In the seminal work of Wiegel (1960) the Author formulated the theory for the study of the wavebreaker performance, quantified through the analysis of the wave transmission past vertical wave barriers. He compared his analytical solution with experimental data finding a good agreement between theory and experiments. The "Wiegel theory" has been widely adopted for design and innovation in the coastal engineering field. On the other hand, the above-mentioned theory tends to overestimate the transmission coefficient as the water depth increases (deep water conditions) and underestimates the coefficient as the water depth decreases in shallow water conditions. Bollmann (1996) proposed a modified power transmission theory that takes into account the effect of partial wave reflection and obtained a lower transmission coefficient compared to the Wiegel theory. In addition, these theories do not take into account the influence of the FB oscillation which produces a significant impact on the wave's energy reflection and dissipation. The FB displacement allows the passage of a larger amount of energy behind it resulting in a less effective behavior of the wavebreaker, compared to the static configuration.

Traditionally, from a mathematical point of view, the interaction between wave systems and floating bodies has been approached using a simplified approach; namely, taking advantage of the Froude–Krylov assumption, the fully coupled fluid–structure interaction problem is reduced to the analysis of the motion of a rigid body governed by a set of second-order ordinary differential equations (ODE). The hydrodynamic loads are considered as coefficients of the system of ODEs and are typically obtained through laboratory experiments or using the potential flow theory (see, for a comprehensive discussion Newman, 1977). In the case of a single degree-of-freedom system (*i.e.* the FB subject to oscillations in the vertical direction only), the hydrodynamic characteristics of the flow affected by the body motion are taken into account considering three parameters, namely added mass, hydrodynamic damping, and the restoring coefficient. For example, Zheng et al. (2004) used the potential flow theory to develop an analytical method to analyze radiation and diffraction of a wave incident over a rectangular FB.

Laboratory experiments have been widely adopted to study the wavebreaker performance both in static and floating configurations. The experiments can analyze different aspects of FB dynamics, like the influence of the incident wave system (either regular or irregular) on the body motion, the effect of the water depth, the geometrical characteristics, and also the presence of different mooring systems. Among the others, Koutandos et al. (2005) studied the interaction between FB and regular and irregular waves considering large-scale facilities in shallow and intermediate water depth conditions. Peña et al. (2011) performed physical model tests considering four different FB geometries and measured the transmission coefficient, mooring lines tension, and module connectors loads; they found that the hydrodynamic behavior of the pontoon is influenced by its own width more than by cross-section geometry.

Starting from the (Macagno, 1954) formula, Ruol et al. (2013) developed empirical formulations for the estimation of the transmission coefficient for an inverted Π-shape and anchored floating wavebreaker subject to the action of irregular waves. In particular, they introduced a nondimensional parameter, the ratio between the incident wave period and the FB natural period to consider the dynamic behavior of the wavebreaker itself. Recently, the hydrodynamic behavior of a model Π-type FB in heave motion, in intermediate depth water conditions, was studied by Kolahdoozan et al. (2017) and they proposed a novel empirical formulation for the transmission coefficient.

Due to the exponential growth of computer performance, computational fluid dynamic methodologies have recently emerged as a tool to investigate the interaction between a body at sea and a wave system. Yang (2015) used the potential flow theory in conjunction with experiments to calculate the coefficients of reflection and transmission for a rectangular and a Π-shape FB. It was found that the potential flow overestimates the wave reflection coefficient. In contrast, the transmission one is in good agreement with experimental data. However, the potential flow theory is not able to predict the generation of the large vortex structure related to the breaking of the wave over the structure. Recently the numerical solution of the Unsteady Reynolds Averaged Navier Stokes (URANS) equations in conjunction with the Volume Of Fluid (VOF) method is becoming more and more popular for the study of propagation of water waves. This methodology is suited to model the interfacial flow between the two fluids (air and water) and, once used in conjunction with a turbulence model, can reproduce the dissipative behavior of the flow after the passage of the wave under the FB.

Some important numerical experiments adopt this methodology, to evaluate the impact of the wavebreaker shape on its performance (see for example Dentale et al., 2014; Arkal Vittal et al., 2016; Ching-Piao et al., 2016). Recently, Zhang and Duan (2018) used URANS to evaluate the performance of a fixed L type and a rectangular FB. They compared their numerical results with those obtained with the potential theory and by experiments and confirmed the influence of turbulent energy dissipation on the transmitted wave height. There are also studies devoted to the analysis of the mutual interaction between water waves and the dynamical response of wavebreakers, using either laboratory experiments or numerical methods. The numerical study

performed by Rahman et al. (2006) used the Navier–Stokes equations, the VOF, and the porous body model (Hur and Mizutani, 2003) paired with the body motion equation to couple the dynamic response of a submerged and moored floating breakwater. The solution of the Navier–Stokes equations in conjunction with VOF and the dynamic mesh technique has become a popular numerical tool to simulate the complex non-linear interaction between water waves and FBs. For example Zhan et al. (2017) analyzed the hydrodynamic response of inversed model T-type FB under regular and irregular wave conditions. Also, numerical and experimental studies focused on the analysis of various types of prototype wavebreakers with different geometry and the influence of the mooring system; the studies above mentioned focused on small-scale wavebreakers. The number of variables that affect the wavebreaker performance, as found by Gesraha (2006), leads to scalability issues when moving from the model to the full scale. To summarize, several studies are present in the literature aimed at the evaluation of the coefficients of transmission and reflection of wavebreakers. Most of them, of an experimental nature, are relative to both static and floating configurations and considered irregular waves. Numerical studies are also present in literature focused on the analysis of wavebreakers both in static and in floating configuration.

In the present paper, we study the behavior of two wavebreakers, a rectangular one and a Π-shape one respectively. The study is carried out numerically, using the URANS methodology discussed above. This research focuses on a full-scale FB, eliminating the scale effects, and emphasizes the differences between the static and the floating configurations. In particular, we focus on the influence of FB movements on the reflective and dissipative mechanisms which play a very important role in the wavebreaker performance. Further, we validate our numerical model against analytical and empirical formulations to show that our numerical method can be applied in a wide range of applications. First, we analyze the problem of static wavebreakers and we compare our results with those obtained with the (Wiegel, 1960) theory and with the modified power transmission theory of Bollmann (1996). Successively we extend the analysis to the floating configuration, in which the body is free to move along the vertical direction in response to the action of the waves. In the floating configuration, the motion of the body is coupled with the fluid dynamics field, through a monolithic explicit solver. Successively, we compare the numerical displacement of the FB with the analytical solution of the governing equation of a rigid body subject to regular wave load. In particular, we consider the second-order ordinary differential equation (ODE) in which the hydrodynamic coefficients, namely the added mass, the damping term, and the restoring spring coefficients are evaluated using our numerical experiments.

We then analyze the response of the wavebreakers in terms of reflection, dissipation, and transmission coefficients and also, the results are compared with the formulas proposed by Macagno (1954) and Ruol et al. (2013) and with the results of the experimental study of Kolahdoozan et al. (2017). Finally, we discuss how the floating configuration behaves compared to the fixed one. In our study, we focus on the case of regular wave systems. The decision to use regular sea wave systems for this study was based on the need to identify the energy transfer and the dissipation mechanism under controlled wave conditions. A future study may investigate a more realistic situation under irregular sea conditions.

The paper is structured as follows: Section 2 contains a description of the mathematical model; Section 3 contains the numerical method; In Section 4 we report the numerical aspects; Section 5 is dedicated to the description and analysis of the results and finally concluding remarks are in Section 6.

2. The mathematical method

We consider a two-phase system composed of air and water and solve the URANS numerically. Both phases are treated as incompressible Newtonian fluids. The free surface is modeled using the volume of fluid (VOF) and therefore an additional transport equation is considered. In the floating configuration, the FB is treated like a rigid body with a Single Degree of Freedom (SDOF) in the vertical direction and its motion is described by the momentum equation. Finally, the coupling between the fluid flow and the motion of the body is simulated through a monolithic and explicit Fluid–Structure Interaction (FSI) algorithm.

2.1. Equations for the fluid motion

The equations governing the unsteady motion of an incompressible Newtonian fluid in the turbulent regime are the Unsteady Reynolds Averaged Navier–Stokes equations. When using a dynamic mesh that deforms in time, the equation set reads as:

$$\frac{\partial(u_i - u_{m,i})}{\partial x_i} = 0 \tag{1}$$

$$\rho\left(\frac{\partial u_i}{\partial t} + \frac{\partial u_i(u_j - u_{m,j})}{\partial x_j}\right) = -\frac{\partial p}{\partial x_i} + (\mu + \mu_t)\frac{\partial^2 u_i}{\partial x_j \partial x_j} - \rho g \delta_{i,3} + f_{\sigma,i} \tag{2}$$

where u_i is the Reynolds averaged velocity component along the x_i-direction, p is the Reynolds averaged pressure, ρ is the density of the fluid, μ and μ_t are, respectively the dynamic molecular and eddy viscosities, $f_{\sigma,i}$ is the surface tension, g is the gravitational acceleration and $u_{m,i}$ is the component of the mesh deformation rate along the x_i direction. The density is not constant in the domain, as we consider the fluid composed of two phases whose variations are evaluated through the following weighted average equation:

$$\rho = \alpha\rho_w + (1 - \alpha)\rho_a \tag{3}$$

in Eq. (3), ρ_w and ρ_a are, respectively, the water and air density and α is a scalar equal to 1 in the water phase and 0 in the other one. The surface tension is given by:

$$f_{\sigma,i} = \sigma k \frac{\partial \alpha}{\partial x_i} \tag{4}$$

where σ is the surface tension and k is:

$$k = -\frac{\partial n_i}{\partial x_i} = -\frac{\partial}{\partial x_i}\left(\frac{\partial \alpha / \partial x_i}{\|\partial \alpha / \partial x_i\|}\right) \tag{5}$$

To detect the position of the free surface, we solve the following transport equation:

$$\frac{\partial \alpha}{\partial t} + \frac{\partial u_i \alpha}{\partial x_i} = 0 \tag{6}$$

Finally the motion of the computational mesh, needed to simulate the FB configuration, is given by $dv_{m,i}/dt$ in which $v_{m,i}$ is the mesh displacement along the x_i direction obtained form the solution of the Laplace equation:

$$\frac{\partial^2 \gamma v_{m,j}}{\partial x_j \partial x_j} = 0 \tag{7}$$

which has as boundary conditions $v_{m,i} = v_i$, meaning that, at the interface, the mesh displacement of the fluid phase must be equal to that of the solid wall.

2.2. The regular wave theory

There are sveral theories describing the propagation of water waves. They rely on the assumption of irrotational and inviscid flow, such that the velocity field can be expressed through the use of a potential function. The shape of the free surface and the velocity and pressure fields depend on the wave height H, the period T, the length λ of the wave, and the depth h of the water column. Fig. 1 depicts the range of application of different theories, depending on the value of two non-dimensional groups, namely H/gT^2 and h/gT^2.

In this study, we simulate regular wave systems that can be obtained analytically using the second-order Stokes-wave theory. These waves develop over intermediate depths for moderate wave amplitudes (see

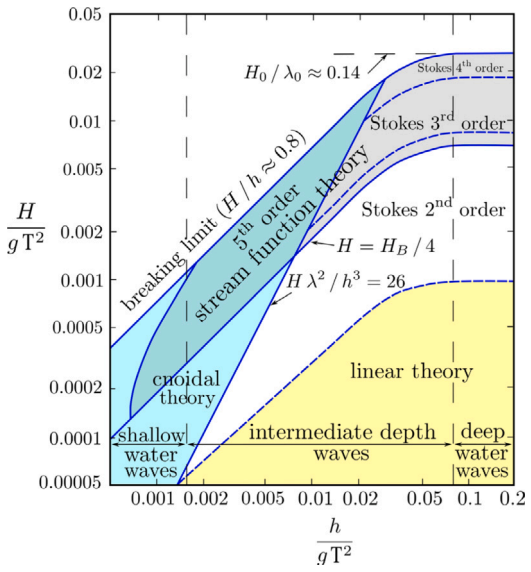

Fig. 1. Range of application of wave theories.
Source: Figure from Huntley (1977).

Fig. 1). The free-surface elevation and the velocity components in the $x_1 \equiv x$ and $x_2 \equiv z$ directions respectively, are:

$$\eta = \frac{H}{2}\cos(\theta) + k\frac{H^2}{4}\frac{3-\sigma^2}{4\sigma^3}\cos(2\theta) \tag{8}$$

$$u = \frac{H}{2}\omega\frac{\cosh(kz)}{\sinh(kh)}\cos(\theta) + \frac{3}{4}\frac{H^2\omega k\cosh(2kz)}{4\sinh^4(kh)}\cos(2\theta) \tag{9}$$

$$w = \frac{H}{2}\omega\frac{\sinh(kz)}{\sinh(kh)}\sin(\theta) + \frac{3}{4}\frac{H^2\omega k\sinh(2kz)}{4\sinh^4(kh)}\sin(2\theta) \tag{10}$$

where $\sigma = tanh(kh)$ and the wave phase is $\theta = kx - \omega t$ with $k = 2\pi/\lambda$ the wave number and $\omega = 2\pi/T$ the angular frequency.

2.3. Equation for the body motion

The motion of a rigid body is governed by the second Newton's Law:

$$F_i = \frac{d\ m_i}{dt} \tag{11}$$

$$T_i = \frac{d\ H_i}{dt} \tag{12}$$

where F_i and m_i are, respectively, the x_i components of the force over the body and the linear momentum vector, and, similarly, T_i and H_i are the x_i components of the torque and angular momentum over the body.

The fully hydrodynamic approach requires coupling the hydrodynamic part with that solving the equation of motion of the body. The coupling is described in a successive part of the paper. Traditionally, a simplified, still effective, approach has been followed in literature, based on the Froude–Krylov assumption on the interaction between the wave system and the body. The problem is described mathematically by a system of second-order ordinary differential equations, whose coefficients represent hydrodynamic actions to be evaluated *apriori* according to well-established theories or laboratory experiments. Considering a floating rigid body with a Single Degree Of Freedom (SDOF) along the vertical direction subject to regular wave loads, the study can be performed considering a single ordinary differential equation representative of the heave motion:

$$(m+a)\ddot{v_z} + b\dot{v_z} + cv_z = F_w \tag{13}$$

where v_z is the vertical displacement, m is the mass, a is the added mass, b is the hydrodynamic damping coefficient, $c = \rho g A_w$ is the restoring coefficient with A_w the water plane area and F_w is the periodic wave load (Froude–Krylov force) in the vertical direction.

The motion of the floating body generates two hydrodynamic forces respectively identified by the terms $a\ddot{v_z}$ and $b\dot{v_z}$. In particular, the displacement of the body generates waves that propagate away from it in the radial direction. The resulting waves carry energy away from the body and have a dampening effect proportional to the velocity of the body and it is identified by the hydrodynamic damping coefficient b. The other hydrodynamic effect is caused by the acceleration of the particles near the body, and it is considered as an added mass a in the equation. The restoring coefficient is due to the Archimedes Law. Finally, the wave load is individuated by the Froude–Krylov force (Journée and Massie, 2001), which follows from the integration of the pressure field over the body surface. In general, to take into account the diffraction of the waves, a correction of the Froude–Krylov force is given by the following equation:

$$F_w = a\ddot{\eta}^* + b\dot{\eta}^* + c\eta^* \tag{14}$$

where $a\ddot{\eta}^*$ e $b\dot{\eta}^*$ are the correction factors due to the diffraction of the wave by the presence of the body. The reduced wave is given by the following:

$$\eta^* = \eta_a e^{-kT_b}\cos(\omega t) \tag{15}$$

where T_b is the draft of the body, ω is the angular frequency of the incident wave and η_a is the amplitude of the wave.

Finally the final form of the Froude–Krylov force is:

$$F_w = F_a\cos(\omega t + \epsilon_{F\eta}) \tag{16}$$

where the amplitude and the phase of the force are given by:

$$\frac{F_a}{\eta_a} = e^{-kT_b}\sqrt{[c-a\omega^2]^2 + [b\omega]^2} \tag{17}$$

$$\epsilon_{F\eta} = \arctan\left[\frac{b\omega}{c-a\omega^2}\right] \quad with: \quad 0 \le \epsilon_{z\eta} \le 2\pi \tag{18}$$

Eq. (13) assumes the following form:

$$(m+a)\ddot{v_z} + b\dot{v_z} + cv_z = F_a\cos(\omega t + \epsilon_{F\eta}) \tag{19}$$

with general solution given by:

$$v_z = v_{z,a}\cos(\omega t + \epsilon_{z\eta}) \tag{20}$$

where:

$$\frac{v_{z,a}}{\eta_a} = e^{-kT_b}\sqrt{\frac{[c-a\omega^2]^2 + [b\omega]^2}{[c-(m+a)\omega^2]^2 + [b\omega]^2}} \tag{21}$$

$$\epsilon_{z\eta} = \arctan\left[\frac{-mb\omega^3}{(c-a\omega^2)[c-(m+a)\omega^2] + [b\omega]^2}\right] \quad with: \quad 0 \le \epsilon_{z_\eta} \le 2\pi \tag{22}$$

In the present study, we apply both methodologies. Specifically, first, we numerically solve Eq. (11), where the forces are directly evaluated from the fluid dynamic field, to obtain the body displacement, which in turn influences the fluid motion. We use the already mentioned Fluid–Structure Interaction (FSI) algorithm. In this way, we take into account the viscous and rotational effects of the fluid flow, which is neglected in the simplified ODE model. Successively we use the ODE model with coefficients found from the fully hydrodynamic approach and compare them with those available in literature.

3. The numerical method

The fluid motion is described by the URANS equations, which provide a two- or three-dimensional time-dependent representation of the turbulent flow field; the dissipative character of the flow due to

turbulence is here taken into account by the use of the $k-\epsilon$ turbulence model, which requires the solution of two additional partial differential equations, one for the turbulent kinetic energy (k) and the other one for its dissipation rate (ϵ). The equation set is solved using the PISO algorithm, as implemented in the open-source numerical framework OpenFoam. We use the version OpenFOAM-v22.06, with the extended tool olaFlow. The time advancement of the algorithm for the fluid motion is carried out using the implicit first-order (Euler) scheme. For spatial discretization, we use the second-order Gauss integration scheme with a linear interpolation. Further, for the Laplacian term, we use the Gauss integration scheme with a correction of the skewness. In this way, we avoid numerical instabilities triggered by excessive deformation of the mesh arising in the floating body configuration. We use the PCG method to solve the linear systems for the velocity field, using a smoother based on the Gauss–Seidel scheme. Finally, we use two non-orthogonal corrector steps, because of the mesh deformation occurring in the floating case. Overall, the algorithm is first-order accurate in time and second-order accurate in space. The body motion and the fluid flow interact through an explicit and monolithic algorithm; in particular, we use the *sixDofRigidBodyMotion* solver implemented in OpenFOAM. We use a time-step equal to 0.001 s which ensures a Courant condition, $Co < 1.0$.

4. Numerical setup

In the present paper, we study the hydrodynamic behavior of static and floating wavebreakers for different regular monochromatic waves. The control parameters are the wave height H and period T, the depth of the seabed h, and the shapes of the breakers;

Specifically, we study 5 sets of regular waves in intermediate-depth water conditions (Table 1). First, we compare the time record of the free surface pattern with the analytical solution, in order to verify the reliability of the algorithm for the generation and propagation of the waves. Afterward, we study the dissipative behavior of the rectangular and of the Π-shape wavebreakers, considered fixed in space, when subject to the action of the regular waves of Table 1. Finally, we analyze the floating wavebreakers, considered free to move along the vertical direction. The study is carried out for a *2D* configuration, representative of wavebreakers elongated along the cross-stream direction. We use a two-dimensional rectangular domain with a length $L = 200.00$ m in the x-direction and height $A = 20.00$ m in the z-direction with a water depth of $h = 9.0$ m. The wavebreakers are placed at the center of the domain. The rectangular wavebreaker has a length $B = 3.00$ m in the x-direction and the height is $D = 2.40$ m in the z-direction; the draft of the wavebreaker is $d = 1.9$ m under the wavebreaker roof. The dimension of the wavebreakers herein considered is typical of engineering applications.

The Π-shape wavebreaker is composed of a rectangular box and two vertical appendages placed at the edges of the main box. It has a length $B = 3.00$ m in the x-direction and height $D = 2.40$ m in the z-direction as for the rectangular case; the draft of the wavebreaker is $d = 1.9$ m. The two plates have a thickness $t = 0.22$ m and height $h_p = 0.72$ m. The schematic of the wavebreakers is in Fig. 2.

To ensure adequate numerical resolution of the hydrodynamic field, a convergence study was carried out considering several grids. The generation of the mesh is driven by the need to resolve adequately the water–air interface. As described by Zhang and Duan (2018), near the free surface the horizontal dimension of the grid cells must be $\sim 1/100$ of the wavelength, while the vertical dimension must be $\sim 1/60$ of the wave height. Table 2 reports the dimensions of the mesh and in Fig. 3 we show a zoom of the mesh near the wavebreaker.

As boundary conditions, we set the generation of a second-order Stokes wave at the inlet, while at the outlet we set the absorption boundary condition. On the upper plane, we set the atmospheric boundary condition which allows air to pass through. On the bottom plane, we set the no-slip condition. Since OpenFoam is inherently three-dimensional, on the front and back of the computational domain we set the empty condition which mimics a two-dimensional case. On the wavebreaker, we set the moving wall velocity, meaning that the velocity of the fluid is the same as that of the body. In the static body configuration, this condition reduces to the no-slip one.

Table 1
Parameters of the waves.

Wave height H [m]	Wave length λ [m]	Wave period T [s]
0.5	19.03	3.5
0.6	21.72	3.75
0.7	24.49	4.0
0.8	27.32	4.25
0.9	30.16	4.5

Table 2
Parameters of the mesh.

$min(\Delta x/L)$	$min(\Delta z/A)$	n° of cells	n° of points
0,0001	0.00008	4.959.500	9.940.840

5. Results and discussion

Here, we first discuss the generation and propagation of the waves in the domain and compare the numerical results with the available analytical ones. Successively, we consider the wavebreakers in the static body configuration and analyze the transmission coefficient for the rectangular and Π-shape wavebreakers. Finally, we study the case of FBs and quantify the differences concerning the previous case in terms of transmission and reflection coefficients.

5.1. Validation of the generation and propagation of waves

We analyze the reliability of the extended tool olaFlow for the generation and propagation of the waves presented above. The wave herein generated is well described by the second-order Stokes theory. We record in time the free surface pattern at the beginning of the water channel, 0.1 m from the wave maker, and we compare the numerical results with the analytical ones. In (Fig. 4) we show the time record of the non-dimensional wave elevation Z/H versus the non-dimensional time tU/λ where λ is the wave length, $U = \lambda/T$ is the wave celerity and T is the wave period. We report the results for one wave only, because, in non-dimensional form, the waves herein are considered to collapse onto a single curve. From the right panel on Fig. 4 we observe that the maximum relative error between numerical and analytical results amounts to about 5.8%. The relative error is calculated as:

$$\epsilon_i = \left| \frac{\sum_{j=1}^{N_i} |Z_{j,i}| - \sum_{j=1}^{N_i} |\tilde{Z}_{j,i}|}{\sum_{j=1}^{N_i} |\tilde{Z}_{j,i}|} \right| 100$$

where Z_i is the ith wave elevation and $\tilde{Z}_i$ is the analytical one.

5.2. Analysis of the wavebreakers in the fixed body configuration

In this section, we present the numerical results of the transmission coefficient of the wavebreakers, in the fixed body configuration. When the incident wave impacts the wavebreaker, part of the wave energy is reflected back, part is transmitted downstream and part is dissipated by the swirling and turbulent motion of the fluid. Therefore, the height of the transmitted wave is smaller than that of the incident one. The transmission coefficient is defined as the ratio between the heights of the transmitted and the incident wave $C_t = H_t/H_i$. This parameter is an indicator of the behavior of the wavebreaker. Simplified engineering

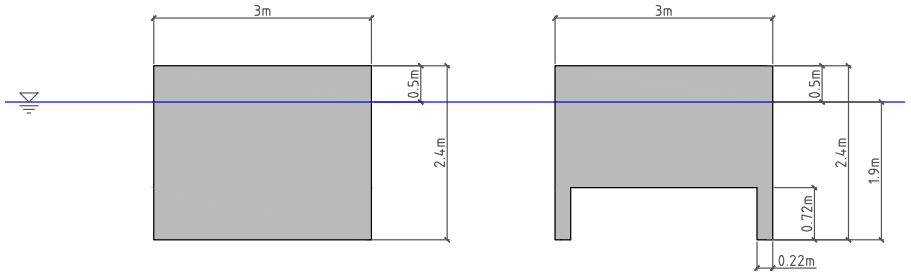

Fig. 2. Schematic of the wavebreakers: left panel, rectangular shape; right panel, Π-shape.

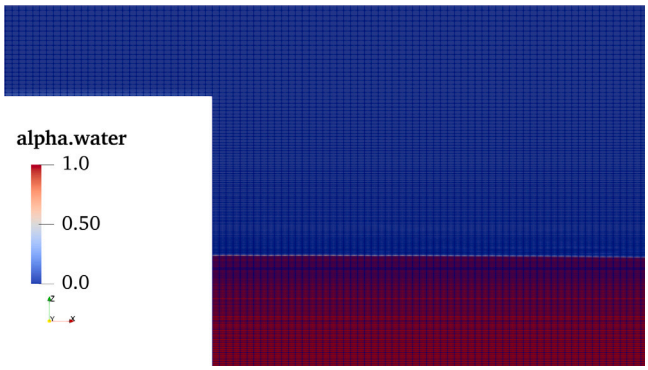

Fig. 3. View of the mesh near the wavebreaker.

formulations are available for a first rough estimation of the transmission coefficient. Among the others, the (Wiegel, 1960) formula is valid for surface-piercing thin barriers:

$$C_t = \sqrt{\frac{\frac{4\pi(h-d)/\lambda}{sinh(4\pi h/\lambda)} + \frac{sinh(4\pi(h-d)/\lambda)}{sinh(4\pi h/\lambda)}}{1 + \frac{4\pi h/\lambda}{sinh(4\pi h/\lambda)}}} \tag{23}$$

where h is the depth of the water column and d is the draft of the submerged part of the structure. The formula is valid under the assumption of the linear wave theory, discussed above. In addition, we compare our numerical results with those obtained with the method of Bollmann (1996), which extends the Wiegel analysis considering the effect of the reflected wave. The equation for the transmission coefficient developed by Bollmann (1996) is the following:

$$C_t = \frac{2T_f}{1+T_f} \tag{24}$$

where T_f is equal to:

$$T_f = \frac{2k(h-d) + sinh(2k(h-d))}{2kh + sinh(2kh)} \tag{25}$$

we calculate the transmission coefficient when the wavebreaker is subject to 5 sets of regular second-order Stokes waves. The simulations were run for a nondimensional time $t/T_i > 13$, where T_i is the wave period for each wave. It has to be mentioned that in the case of wave systems hitting a body, the wave upward is a composition of the incident one and the reflected one. So, a methodology must be used to separate the two contributions for the correct evaluation of the transmission coefficient. Hereafter we describe the methodology for the case of the rectangular fixed wavebreaker when subject to the wave with a height of 0.5 m. The methodology remains the same for the other cases investigated in the paper.

In Fig. 5 we report the time record of the wave elevation at $x_1 = 90$ m (at a nondimensional distance from the obstacle ($L_{nd} = \frac{L}{2} - x_1)/B = 3.33$) and the analytical one together with the spectra of the two signals. We can see that the wave height in the upward position is not as regular as the pure incident wave (Fig. 5, left panel). The wave system is, in fact, partially reflected by the wavebreaker, resulting in a composition of different waves with different frequencies and amplitudes, as evidenced in the right panel of Fig. 5. To separate the contributions of the incident wave from the reflected one, we adopt the two-point method of Yoshimi and Yasumasa (1976). With this purpose, we record the wave elevation at two probes, respectively $x_1 = 90$ m ($L_{nd} = 3.33$) and $x_2 = 96$ m ($L_{nd} = 1.33$), such that the distance between the probes (Δx) is set out of the range $0.4\lambda < \Delta x < 0.6\lambda$, where λ is the wave length, as recommended by Michael (1991). We record the amplitudes (A_1 and A_2) as the difference between the minimum and maximum value, and we calculate the difference in phase (δ) of the two time signals. Finally using the following equations we calculate the heights of the incident (H_i) and reflected (H_f) wave as:

$$H_i = \frac{1}{sin(\Delta)}\sqrt{A_1{}^2 + A_2{}^2 - 2A_1A_2cos(\Delta+\delta)} \tag{26}$$

$$H_r = \frac{1}{sin(\Delta)}\sqrt{A_1{}^2 + A_2{}^2 - 2A_1A_2cos(\Delta-\delta)} \tag{27}$$

where $\Delta = k\Delta x$, with k the wave number. For the post-processing analysis we consider the time window in the range $45U/\lambda - 60U/\lambda$ as shown with the gray area in Fig. 5. In this case, we found that the wave heights are 0.46 m and 0.41 m for the incident and reflected wave, respectively; consequently, the reflection coefficient is equal to $C_r = H_r/H_i = 0.89$. The methodology has been applied to the other cases and the results are summarized in the right panel of Fig. 6.

We carried out the simulations for the rectangular and the Π-shape body, considering the five II-order Stokes waves discussed above. To estimate the transmission coefficient we recorded the wave elevation at $x_3 = 110$ m, namely 3.33 body lengths downstream the wavebreaker. The transmission coefficients obtained in our study are compared with literature data in Fig. 6. Specifically, the figure contains the values obtained with the engineering (Wiegel, 1960) formula, the modified Wiegel formula (Bollmann, 1996), and our numerical results. Finally, the dissipation coefficients (reported in the lower panel of Fig. 6) are identified through the following energy balance:

$$E_i = E_d + E_r + E_t$$

where E_i represents the energy of the incident wave, E_d indicates the dissipated energy, E_r is the reflected wave energy and E_t denotes the transmitted wave energy. It should also be noted that wave energy is proportional to the square of its height and can be calculated as $E = \frac{1}{8}\rho g H^2$. As a result, the following equation applies:

$$H_i^2 = H_d^2 + H_r^2 + H_t^2$$

finally, after dividing by H_i, we obtain:

$$C_t^2 + C_r^2 + C_d^2 = 1$$

and

$$C_d = \sqrt{1 - C_t^2 - C_r^2}$$

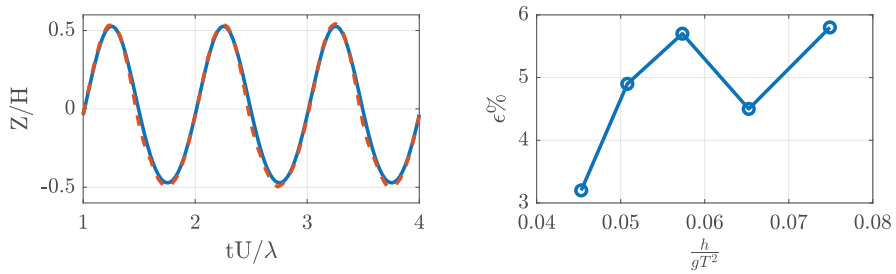

Fig. 4. Left panel: time record of the non-dimensional free surface elevation versus non-dimensional time obtained in numerical simulations (dashed line) and from the second-order Stokes theory (solid line). Right panel: relative error for each wave.

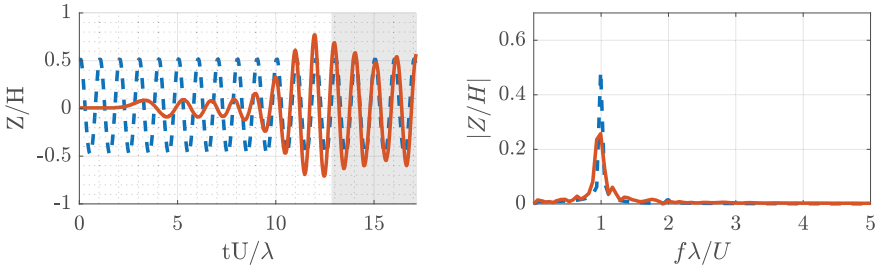

Fig. 5. Left panel: time record of the wave elevation at $x_1 = 90$ m (orange solid line), and the analytical one (dashed line); right panel: spectra of the time signals. Wave height equal to 0.5 m. The gray area refers to the time window used for post-processing analysis.

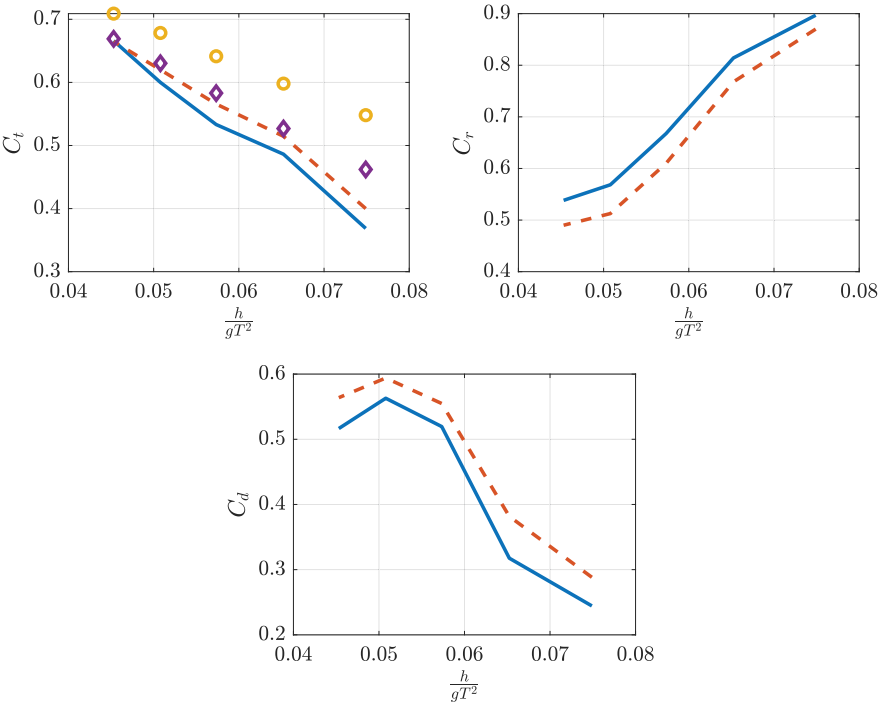

Fig. 6. Top-left panel: transmission coefficients obtained with: the Wiegel formula (dots); the modified Wiegel formula (diamond marks); our numerical results for the rectangular wavebreaker (solid line) and the Π-shape wavebreaker (dashed line). Top-right panel: reflection coefficients obtained with our numerical simulations for the rectangular (solid line) and Π-shaped wavebreaker (dashed line) respectively. Lower panel: dissipation coefficient obtained with our numerical simulations for the rectangular (solid line) and Π-shaped wavebreaker (dashed line) respectively.

We carried out numerical simulations while keeping the water depth constant, varying the wave height and the period of the wave in the range of intermediate water depth conditions. It is well-known that the (Wiegel, 1960) formula tends to overestimate the transmission coefficient in deep water conditions and, on the other hand, to underestimate it in nearly shallow water conditions. Therefore, to highlight this fact we plot the transmission coefficient as a function of the non-dimensional parameter h/gT^2, where the variable is the wave period (T), consistently to Fig. 1 reported in Huntley (1977). The analysis of Fig. 6 (left panel) shows that the Wiegel formula as well as the modified Wiegel formula overestimate the transmission coefficient when approaching the deep water conditions (moving to the right in the plot).

Fig. 6 (left panel) also shows that the transmission coefficient decreases with decreasing the wave period and consequently the wave length. This increased efficiency has to be associated to the increased

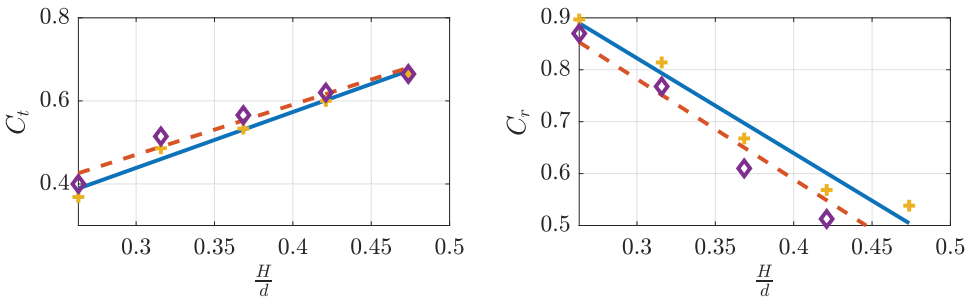

Fig. 7. Left panel: transmission coefficients obtained with: our numerical results for the rectangular wavebreaker (crosses dot), the relative linear regression (solid line), the Π-shape wavebreaker (diamonds dot), and the relative linear regression (dashed line). Right panel: reflection coefficients obtained with our numerical simulations for the rectangular wavebreaker (crosses dot), the relative linear regression (solid line), the Π-shape wavebreaker (diamonds dot), and the relative linear regression (dashed line).

wave reflection occurring when the wave length decreases (see Fig. 6, right panel). In addition, we can see that the rectangular wavebreaker is more efficient than the Π-shape one, since the latter appears less reflective (by about the 6.7%), compared to the rectangular one (right panel of Fig. 6).

Both wavebreakers are more reflective with the wave height equal to 0.5 m (see the point on the right side of the right panel of Fig. 6) and the reflection decreases as the wave height increases. Actually, if the draft is much smaller than the wave height ($d \ll H$), the reflection goes to zero; conversely if the draft increases while maintaining a constant wave height, the reflection increases to a maximum value, corresponding to complete reflection occurring for the draft to reach the bottom of the water column. As expected, the transmission coefficient exhibits the opposite trend. The analysis of Fig. 7 suggests the existence of a quasi-linear relationship between the transmission and reflection coefficients and the parameter H/d. Specifically, the linear regression equations are the following:

$C_t = 1.35\frac{H}{d} + 0.04$ for the rectangular wavebreaker;

$C_t = 1.21\frac{H}{d} + 0.11$ for the Π-shaped wavebreaker;

$C_r = -1.83\frac{H}{d} + 1.37$ for the rectangular wavebreaker;

$C_r = -1.93\frac{H}{d} + 1.36$ for the Π-shaped wavebreaker;

It is a widely acknowledged fact that the Π-shape wavebreaker is more effective in dissipating energy than the rectangular one. In fact, in the bottom panel of Fig. 6, we observe that the Π-shape wavebreaker is more dissipative, on average by around 10.3%, compared to the rectangular one. To understand the differences in energy dissipation for the two wavebreakers, we examined the mean turbulent viscosity field at four different phases of the wave period for both wavebreakers subject to waves with a height of 0.5 m, as shown in Fig. 8. The Π-shape wavebreaker exhibits a level of turbulent viscosity higher than the other wavebreaker throughout all phases of the wave cycle, providing further evidence of its more dissipative behavior. The analysis of Fig. 6 also shows a non-monotonic behavior of the dissipation, with a maximum for the wave height equal to 0.8 m, a quite similar behavior was found by Zhang and Duan (2018). The main dissipation mechanism is due to the generation of turbulent structures. This generates more turbulent kinetic energy and a higher value of the turbulent viscosity which subtracts energy from the mean flow. As the height of the wave varies, the length scale of the mean flow varies accordingly. For lower wave heights, dissipation is low since the length scale of the mean flow is smaller than the draft of the wavebreaker. As wave height increases, the length scale of the mean flow becomes comparable to the draft of the wavebreaker, resulting in higher dissipation. However, if the length scale of the wave exceeds the draft of the wavebreaker, its breaking efficiency decreases, leading to lower dissipation characteristics. In conclusion, the Π-shape wavebreaker is, on one side, more efficient in dissipating wave energy, but, on the other side, it is less efficient in reflecting waves, leading to higher transmission of wave energy and lower efficiency compared to the rectangular one. Our results show that for the cases herein considered the wave reflection plays a role much more important than energy dissipation in the process of wave transmission behind the obstacle.

5.3. Analysis of the floating wavebreakers

Here we analyze the floating configuration of the wavebreaker, treated as a rigid body with a SDOF in the vertical (z) direction. To assess the numerical method we perform comparisons between the numerical displacement and the analytical one (Eq. (20)) when the FB is subject to the regular waves of Table 1. First, we need to evaluate the hydrodynamic coefficients of the FB to resolve analytically Eq. (20). In general, the added mass and the damping coefficients for an arbitrary geometry are not easy to calculate, due to the non linear characteristics of the fluid motion around the body. Moreover, both coefficients depend on several parameters, as found by Gesraha (2006) by the use of the Π Theorem; among the others, the period of oscillation is the most important control parameter. In this study, the hydrodynamic parameters are kept constant while the wave period is varied as in Table 1. This simplification is supported by the fact that the ratio between the fundamental period of oscillation and that of the incident wave, is in the range $0.94 - 1.23$, so small variations of the coefficients are expected. It is noted that the added mass coefficient, for heave oscillation, is qualitatively constant in a wide range of forcing periods as discussed in Gesraha (2006). An approach for the identification of these parameters is the experimental one where a scale model is left free to oscillate, starting from a non-equilibrium position (free decay test). Here we perform this test using numerical experiments. We set the FB in a non-equilibrium position, we let it free to oscillate and we record the displacement of the center of mass. From the typical damping oscillation behavior we can calculate the period of free oscillation T_h and the damping coefficient ν. Further, the relationship presented below, between the free oscillation angular frequency and the damping coefficient allows us to calculate the added mass a and the hydrodynamic damping b as:

$$2\nu = \frac{b}{m+a}$$

$$\omega_0^2 = \frac{c}{m+a}$$

We perform two equivalent numerical experiments respectively for the rectangular body and the Π-shape body. The values of the hydrodynamic coefficients for the two wavebreakers are reported in Table 3, whereas the time records of the FBs displacement are in Fig. 9. The figure shows a more rapid decay of the motion for the rectangular body.

From the decay curves, we calculated the damping and added mass coefficients and compared them with those from the literature for a rectangular body (see Vugts, 1968 and Newman, 1977). Specifically, the author presented the aforementioned coefficients as a function of the non-dimensional parameter $\omega\sqrt{(d)/g}$ for some rectangular FBs with different $B/(d)$ ratios, namely 2, 4, and 8. However, there is no literature data available for our specific $B/(d)$ ratio of 1.58, although the data are comparable. Actually, the literature data, for the rectangular FB with $B/(d) = 2$, are $a/\rho B^2 = 0.39$ and $b/\rho B^2\omega = 0.2$, whereas our results are $a/\rho B^2 = 0.45$ and $b/\rho B^2\omega = 0.31$. When we compare the

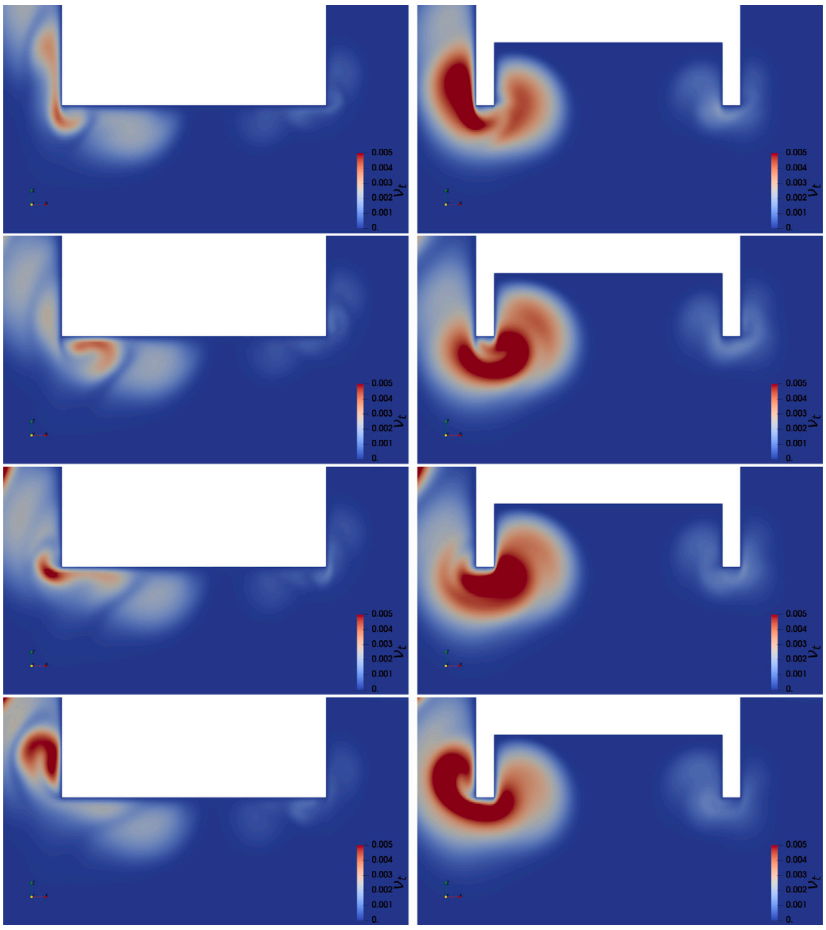

Fig. 8. In these figures we report the mean turbulent viscosity field on the x–z plane when both the fixed wavebreakers are subjected to a wave with height equal to 0.5 m; From the top to the bottom the non dimensional time is: $15.71\,T$; $15.71\,T + \frac{T}{4}$; $15.71\,T + \frac{T}{2}$; $15.71\,T + \frac{3T}{4}$.

Table 3
Hydrodynamic coefficients for the rectangular and Π-shaped FBs.

Hydrodynamic coefficients	Formula	Rectangular FB	Π-shaped FB
Period	T_h	3.65 [s]	3.72 [s]
Damping	ν	0.25 [s^{-1}]	0.18 [s^{-1}]
Mass	$m/\rho B^2$	0.63	0.43
Added mass coefficient	$a/\rho B^2$	0.45	0.7
Hydrodynamic damping coefficient	$b/\rho B^2\omega_0$	0.31	0.24
Restoring spring coefficient	$c/\rho g A_w$	1	1

results for the two geometrical configurations of the FB, we can see that the ratio m/a is quite different moving from the rectangular case to the Π-shape one, whereas the sum of the two terms is similar, being equal to 1.08 and 1.13 for the rectangular and Π-shape wavebreaker, respectively. This is due to the fact that, although the mass of the Π-shape wavebreaker is smaller than that of the rectangular one, its particular shape forces a larger volume of water to follow its movement resulting in a substantially larger added mass compared to the rectangular case. Consequently, the fundamental period of oscillation is a little bit higher in the Π-shape wavebreaker. Finally, the damping coefficient is smaller in the Π-shape body compared to the rectangular one. This indicates that the particular geometry of the Π-shape body produces a less intense combination of wave radiation and energy dissipation in comparison with the rectangular body.

Finally, we perform the numerical simulations of the FBs subject to the five regular waves of Table 1. First, we compare the vertical displacement of the FBs obtained using the numerical method with those obtained analytically with the ODE with coefficients calculated from the numerical free decay tests. In Figs. 10 we report the comparison between the analytical displacement and our numerical results for the rectangular (left panels) and the Π-shape FB (right panels), respectively. The comparison is in general very good, showing the ability of the simple analytical models to reproduce the oscillatory behavior of the floating bodies once the coefficients are evaluated. For the rectangular body, the maximum relative error is about 19% for the wave height $H = 0.5$m. For the Π-shape FB the agreement is very good in all cases but for the smaller wave length and height, where the relative error is of the order of 52%. This indicates that, for the Π-shape geometry, the simple use of coefficients found from free-decay tests might be not appropriate in the range of high-frequency waves. Furthermore, it is worth considering that we do not consider the variation of the damping coefficient with the frequency. This may contribute to the disagreement observed for the high-frequency wave. Finally, a slight difference in phase between the analytical and numerical results is found. The analytical solution refers to the steady periodical oscillation, whereas the numerical one, is obtained considering a numerical wavemaker which produces a long transient and overimposition of a large number of harmonics. From a conceptual point of view, the numerical experiment is more similar to the laboratory one than to the simplified analytical solution.

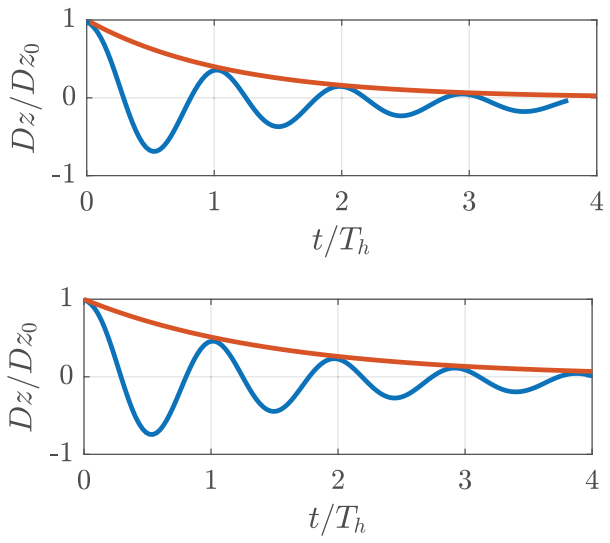

Fig. 9. Time record of the numerical free decay displacement for the rectangular (top panel) and Π-shaped (bottom panel) FBs. The orange lines are the decay curves fitting the numerical data.

Finally, We calculate the transmission coefficients for the two FBs. An analytical formulation of the transmission coefficient for the case of incident regular waves is due to Macagno (1954):

$$k_{tM} = \frac{1}{\sqrt{1 + (kB\frac{\sinh kh}{2\cosh(kh-kd)})^2}}$$

where B and d are the width and the draft of the FB and k is the wave number. The formula was successively improved by Ruol et al. (2013), who, based on results of laboratory experiments, considered an additional nondimensional parameter that takes into account the dynamics of the floating wavebreaker. The experiments were carried out for several Π-shape wavebreakers, anchored with different mooring systems and subject to irregular waves. The above-mentioned parameter, $\xi = T_p/T_{h,R}$, is the ratio between the period of the peak wave period (T_p) and the FB natural period of oscillation ($T_{h,R}$), estimated by the following equation:

$$T_{h,R} = \frac{2\pi}{\sqrt{\frac{g}{d+0.35B}}} = 3.44 \text{ s}$$

the new formula proposed by Ruol et al. (2013) is the following:

$$k_{tR} = \beta(\xi)k_{tM}$$

where:

$$\beta(\xi) = \frac{1}{1 + (\frac{\xi-\xi_0}{\sigma}\exp^{-}(\frac{\xi-\xi_0}{\sigma})^2)}$$

with $\xi_0 = 0.7919$ and $\sigma = 0.1922$.

The equations are valid for a fixed (Macagno, 1954) and an anchored (Ruol et al., 2013) FB. In our numerical simulations, the wavebreakers are free to move in the vertical direction. Despite these differences, we compare the transmission coefficients obtained from our numerical results against literature formulas of Macagno (1954) and Ruol et al. (2013), to have a direct comparison between an empirical formulation, deriving from physical experiments, and the numerical one. In particular in Fig. 11 we report the transmission (left panel) and the reflection (right panel) coefficients. We observe that the performance of the two FBs, when free to oscillate vertically, are very similar to each other. Also, we note that the analytical formula suggested by Macagno (1954) tends to overestimate the transmission coefficient concerning the numerical results. This is because Macagno's theory assumes a linear process and disregards radiated waves. Furthermore, it is widely acknowledged that the (Macagno, 1954) formula provides good qualitative predictions but, in general, is imprecise when compared to experimental data. As discussed by Ruol et al. (2013) Macagno's equation overestimates experimental data by a factor of approximately 1.5 when the ratio of $T_p/T_{h,R}$ is close to 1. It is noted that our results are in very good agreement with the formula of Ruol et al. (2013) when the incident wave period is close to the FB natural one, in particular for the wave height equal to 0.6 m (wave period equal to $T_p = 3.75$ s). For the other wave conditions the numerical model underestimates the transmission coefficient compared to the formulation proposed by Ruol et al. (2013). This can be associated to several factors: first, in our cases the floating bodies are not anchored and free to move vertically, whereas the formula of Ruol et al. (2013) considers several mooring configurations and different degrees of freedom, namely heave, roll, pitch and sway motion. The anchorage may limit the oscillation of the body and alter in a non trivial way the transmission of the wave behind the obstacle; second, we consider regular waves, whereas the empirical formula is based on irregular wave conditions; as a minor effect, the experimental analysis was carried out at a model scale with a factor 1 : 10, and this might underestimate the dissipation due to the high-turbulent flow (see for example Koftis et al., 2006); finally the experiments were carried out considering different models geometry and configurations, and this significantly affects the motion of the body. The qualitative difference between our numerical results and the data obtained using the formula of Ruol et al. (2013) consists in the fact that the results obtained using the formula above mentioned do not show the peak of the transmission coefficient in the resonance condition, which corresponds to the synchronization between the incident and the fundamental period of the oscillation. This is because the wavebreakers are subject to a train of irregular waves with a broadband frequency spectrum, and the mooring system significantly affects the natural period of the body. In general, the analysis of our results suggests that in the monochromatic wave conditions, the resonance region is the critical one, in that the transmission coefficient is the largest compared to the other situations. The comparative analysis of the transmission and reflection coefficients shows that in the off-resonance conditions, a large amount of wave reflection takes place making the FB more efficient. We also analyze the dissipation of the whole system, which is characterized by two fundamental contributions: the dissipation of the mean flow energy due to the turbulent viscosity and the energy absorbed by the body. We can write the following energy balance:

$$\frac{1}{8}\rho g\lambda H_i^2 = \frac{1}{8}\rho g\lambda H_r^2 + \frac{1}{8}\rho g\lambda H_t^2 + \frac{1}{8}\rho g\lambda H_d^2 + \frac{1}{4}((m+a)\omega^2 + c)(z_a)^2$$

Where the incident wave energy is represented by the first term on the right-hand side, the left-hand side comprises the reflected wave energy, the transmitted wave energy, the energy dissipated by the turbulent motion, and the energy absorbed by the body motion. z_a denotes the amplitude of the heave oscillation. Dividing the entire equation by the first term we obtain:

$$1 = C_r^2 + C_t^2 + C_d^*$$

where C_d^* is:

$$C_d^* = C_d^2 + C_s^2 = C_d^2 + \frac{((m+a)\omega^2 + c)}{2\rho g\lambda}(RAO(\omega))^2$$

in which the RAO represents the response amplitude operator defined as :

$$RAO(\omega) = 2z_a/H_i$$

in this way, the dissipation coefficient due to the turbulence is given by:

$$C_d = \sqrt{1 - C_r^2 - C_t^2 - C_s^2}$$

in Fig. 11 we report the whole dissipation coefficient (C_d^*) in Fig. 11.c, the absorption coefficient due to the body motion (C_s) in Fig. 11.d and

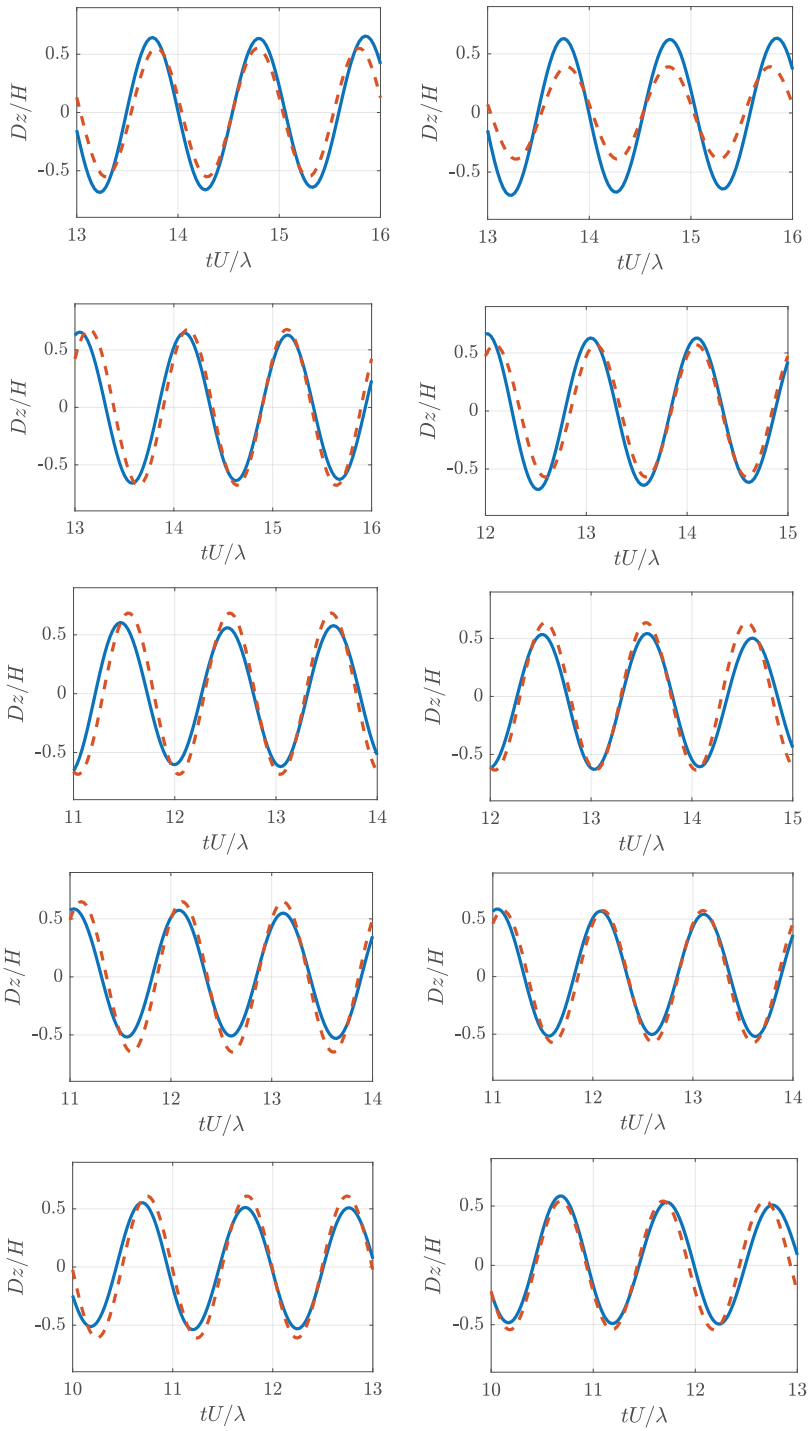

Fig. 10. Comparison between the numerical (blue solid line) and analytical displacement (red dashed line) for the rectangular FB (left panels) and Π-shape FB (right panels). From the top to the bottom: $H = 0.5$ m; $H = 0.6$ m; $H = 0.7$ m; $H = 0.8$ m; $H = 0.9$ m.

the dissipation coefficient (C_d) due only to turbulence, in Fig. 11.e. The reflection affected by the movement of the body shows a non-monotonic behavior. In particular, in the resonance region the reflection is significantly less due to a higher amplitude of the body oscillation. On the other hand, the dissipation of the whole system (Fig. 11.c) presents a monotonic behavior, in fact, the dissipation increases as the wave height decreases. The consistent trend observed in the overall dissipation coefficient is attributed to the absorption of body movements, which increases as the wave height decreases. In addition, as the wave height increases, the frequency decreases and we move towards the lower frequency region of the wavebreaker spectrum (RAO). The FB tends to follow the wave pattern (the shift phase is small) and is therefore unable to absorb much of the wave energy, resulting in less dissipation due to turbulence. As the wave frequency increases towards the resonance region, where the wavebreaker motion is dominated by the damping term (combination of the wave radiation and turbulence dissipation), higher values of the oscillation amplitude and larger shift of phase are observed resulting in a larger amount of energy absorbed by the body motion. On the other hand, when the phase shift and the oscillation amplitude are high, due to the resonance

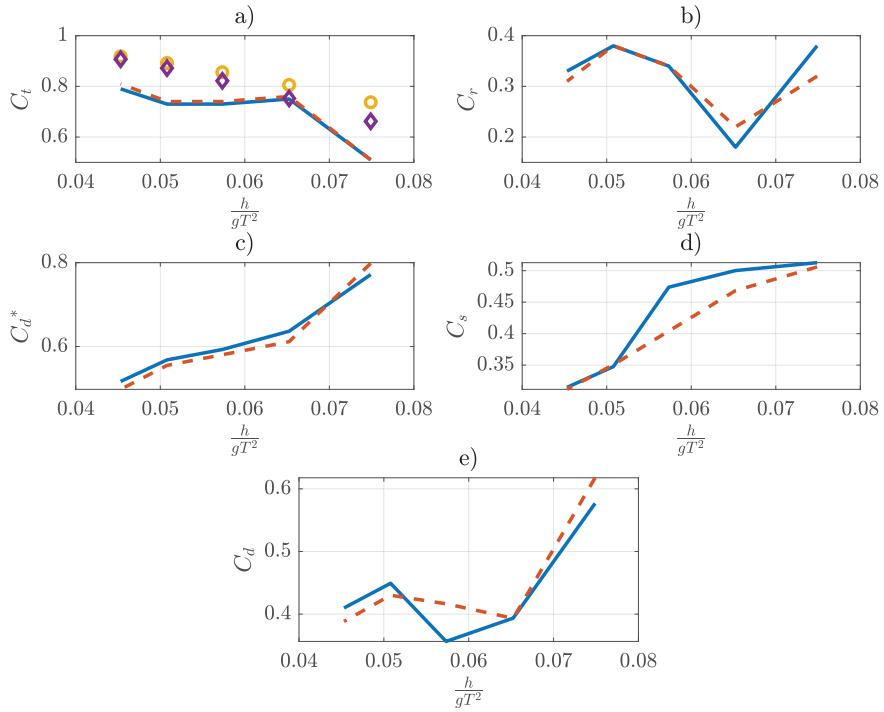

Fig. 11. Panel (a): transmission coefficients obtained with: the Macagno's formula (dots); the Ruol formula (diamond marks); our numerical results rectangular wavebreaker (solid line) and Π-shaped wavebreaker (dashed line). Panel (b): reflection coefficients obtained with our numerical results rectangular wavebreaker (fixed line) and Π-shaped wavebreaker (dashed line). panel (c): dissipation of the whole system (sum of the turbulence dissipation and body motion absorption) obtained with our numerical simulations for the rectangular (solid line) and Π-shaped wavebreaker (dashed line) respectively. Panel (d): dissipation coefficient of the wavebreaker system obtained with our numerical simulations for the rectangular (solid line) and Π-shaped wavebreaker (dashed line) respectively. Panel e): dissipation coefficient (only fluid dissipation) obtained with our numerical simulations for the rectangular (solid line) and Π-shaped wavebreaker (dashed line) respectively.

phenomenon, the generation of swirling structures is more efficient and results in more dissipation due to turbulence.

In other words, in the case of floating configuration, the efficiency of the wavebreaker appears strictly related to its own capacity to reflect part of the wave energy more than to the dissipation of energy due to the sum of turbulence and body motion absorption. This justifies the very small differences between the two geometric configurations.

Finally, for a more detailed comparison with relevant experiments we analyzed our results in view of the relevant experimental campaigns of Ruol et al. (2013) and of Kolahdoozan et al. (2017). In particular (Kolahdoozan et al., 2017) proposed the following novel empirical formula:

$$k_{tK} = \frac{1}{\sqrt{1 + 9.56(\frac{B}{\lambda})^{0.73}(\frac{d}{h-d})}}$$

which is based on their experiments performed in intermediate water conditions, considering a floating Π-type breakwater anchored with lubricated rails and free to move in the vertical direction. In Fig. 12 we present the transmission coefficient obtained by our numerical results referred to the Π-type FB in both static and floating configuration, and considering the empirical formulas by Ruol et al. (2013) and Kolahdoozan et al. (2017) and the regression line, respectively. The (Ruol et al., 2013) formula tends to overestimate the transmission coefficient, although the slope of the lines (around 1.21 for the static configuration and 1.10 for the floating configuration respectively), are in good agreement with the reference one (about 1.15). The use of the (Kolahdoozan et al., 2017) formula tends to underestimate the transmission coefficient in floating configuration and the values are comparable with those obtained in the static configuration, although the lines differ in the slope (around 0.3). The differences between our results and those obtained with the formula of Ruol et al. (2013) may be because their experiments were performed under irregular sea conditions and considering different types of mooring systems which is more appropriate to represent a rigid body with more than one degree of freedom.

The disagreement between our numerical results and the use of the formula of Kolahdoozan et al. (2017) may be associated with the fact that the formula is designed for a range of water depths out of that considered in our study. This might also explain the differences in terms of slopes of the lines of Fig. 12. In any case, our data are within the uncertainty given by the use of the two empirical formulas.

More research is needed to give an explanation to these issues, considering a wide range of water depths and different constraints and degrees of freedom, to better reproduce the physical experiments.

6. Conclusions

In the present paper, we analyzed the hydrodynamic response of a full-scale rectangular and a Π-shape wavebreaker, when subject to regular waves. We considered these geometries at a prototypical scale because are of common use in technological applications. We focused on the performance of the wavebreaker in terms of energy dissipation, reflection, and transmission. The study was carried out numerically, using computational fluid dynamics. We considered two configurations, respectively the static one and the floating body one. In the latter case, the body was considered to move in the vertical direction only. The hydrodynamic field was obtained using the URANS equations with the $k-\epsilon$ turbulence model, and the free surface was modeled using the VOF method. The solver herein employed is OlaFlow, within the OpenFOAM platform. In the case of floating body, its interaction with the fluid flow was taken into account by an explicit and monolithic FSI algorithm. In particular, we used the sixDofRigidBodyMotion solver already implemented in OpenFOAM. Our numerical results were validated considering analytical and empirical formulations, the latter based on massive experimental campaigns.

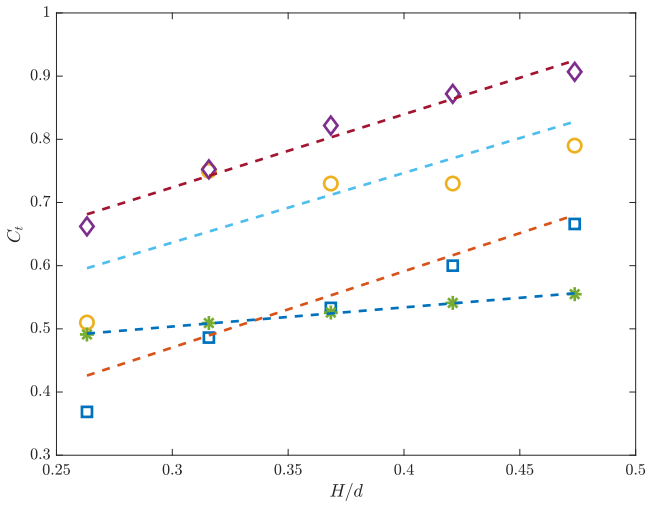

Fig. 12. Transmission coefficient versus the non-dimensional parameter H/d; the dots and square markers are our numerical results referred to the floating and static configuration cases, respectively; The diamond markers are the results obtained by the formula of Ruol et al. (2013); The asterisk markers are the results considering the (Kolahdoozan et al., 2017) formula; The dashed lines are the corresponding regression lines.

Initially, we investigated the generation and propagation of the wave systems and compared numerical results with the available analytical data. We found a good agreement, with an error within 5.8%. Afterward, we considered the presence of the wavebreaker, fixed in space, and we evaluated the transmission coefficient and compared our numerical results with those obtained with the classical formula of Wiegel and with the modified Wiegel formula. The agreement was in general satisfactory. We found that the Π-shape wavebreaker is less reflective and more transmissive and dissipative than the rectangular one, which appears more efficient than the former. In fact, we found that in this situation, wave reflection plays a role much more significant than energy dissipation.

Successively, we performed the analysis of the response of the floating wavebreaker. We recorded the FB heave displacement and we compared our results with those of analytical theory finding a general satisfactory agreement. In particular, we found that using the hydrodynamic coefficients obtained by numerical free decay tests allows us to obtain an accurate evaluation of the heavy motion of the structure when excited by monochromatic waves in a range of frequencies around the resonant one. We also measured the reflected and transmitted waves and calculated the corresponding coefficients. Additionally, by using the energy balance equation and taking into account the energy absorbed by the body motion, we determined the dissipation coefficient associated with turbulence and wave radiation from the body motion. Finally, we compared our numerical results with those of the Ruol et Al. empirical formulation for the transmission coefficient. We found a good agreement with the Ruol at Al. formula when the wavebreaker is in the resonance region. The disagreement found in off-resonance conditions may be since the empirical formulation refers to moored systems in the irregular sea, conditions substantially different from those herein discussed. We found that the motion of the FB has a significant effect on transmission, reflection, and dissipation. In particular, when the wavebreaker is free to move in the vertical direction, a larger amount of the wave energy is transmitted downstream compared to the static case. We found that for the low-frequency waves (higher wave heights) the movement of the body follows the free surface pattern so that the wavebreaker is unable to absorb or reflect a significant amount of wave energy and, also, the dissipation due to turbulence is small. On the other hand, moving towards the resonance region produces a larger amplitude of the body oscillation and shift of phase, resulting in a higher absorption of energy due to the body motion and a greater generation of turbulent structures. Furthermore, we found that the hydrodynamic behavior of the rectangular and the Π-shaped wavebreakers is similar. In fact, in this condition, the efficiency of the wavebreaker seems to be strictly related to its own ability to reflect some of the wave energy, rather than to the dissipation of energy due to turbulence and body motion.

In conclusion, the study shows that the most effective configuration is characterized by a static setup. As freedom of movement expands, which typically occurs in systems moored with chains, the system's performance tends to diminish. The comparison of results of our study with literature formulas, highlights the need for further investigations, extending the numerical analysis herein performed over a wide range of water depth conditions. Also, future analysis should focus on the effect of the mooring system on the oscillatory motion of the FB and the presence of irregular wave systems.

CRediT authorship contribution statement

Giacomo Rismondo: Data curation, Investigation, Methodology, Software, Writing – original draft, Writing – review & editing. **Vincenzo Armenio:** Conceptualization, Formal analysis, Investigation, Methodology, Supervision, Writing – original draft, Writing – review & editing.

Declaration of competing interest

The authors declare that they have no known competing financial interests or personal relationships that could have appeared to influence the work reported in this paper.

Data availability

Data will be made available on request.

Acknowledgements

We thank Eng. Sebastiano Troian for the contribution that he has provided us at the initial stage of the research. The authors acknowledge the support of the Center of Advanced Computing and Modelling at the University of Rijeka for providing the HPC resources.

References

Abhinav, K.A., Collu, M., Benjamins, S., Cai, H., Hughes, A., Jiang, B., Jude, S., Leithead, W., Lin, C., Liu, C., Recalde-Camacho, L., Serpetti, N., Sun, K., Wilson, B., Yue, H., Zhou, B.Z., 2020. Offshore multi-purpose platforms for a Blue Growth: A technological, environmental and socio-economic review. Sci. Total Environ. 734, 138256.

Arkal Vittal, H., Vivek, K.G., Ankit, A., Shivaraj, S.M., 2016. Simulation using computational fluid dynamics (CFD) for semi-circular breakwater during flow over it.

Bollmann, C.A., 1996. Wave interactions with vertical wave barriers. Technical report, Naval Academy Annapolis Md.

Bruce, M.L., 1985. Floating breakwater design. J. Waterw. Port Coast. Ocean Eng. 111 (2), 304–318.

Ching-Piao, T., Ying-Chi, C., Chun-Jen, C., Chang, L., 2016. Simulation of the effect of breakwater on the propagation of solitary waves. J. Mar. Sci. Technol. 24 (4), 12.

Chun-Yan, J., Xiang, C., Jie, C., Zhi-Ming, Y., Atilla, I., 2015. Experimental study of a new type of floating breakwater. Ocean Eng. 105, 295–303.

Cox, R., Beach, Daniel, 2006. Floating breakwater performance-wave transmission and reflection, energy dissipation, motions and restraining forces. In: Proceedings of the First International Conference on the Application of Physical Modelling To Port and Coastal Protection. pp. 371–381.

Dentale, F., Donnarumma, G., Carratelli, E.P., 2014. Numerical wave interaction with tetrapods breakwater. Int. J. Nav. Archit. Ocean Eng. 6 (4), 800–812.

Falcão, A., 2010. Wave energy utilization: A review of the technologies. Renew. Sustain. Energy Rev. 14 (3), 899–918.

Gaythwaite, Johnw, 1987. Floating breakwaters for small craft facilities. Civ. Eng. Pract. 89.

Gesraha, M.R., 2006. Analysis of pi-shaped floating breakwater in oblique waves: I. impervious rigid wave boards. Appl. Ocean Res. 28 (5), 327–338.
Hong, W., Hongbin, X., Peng, L., Jingang, J., Hao, C., Bin, W., 2015. Experimental study on the dissipation characteristics of curtain-type flexible floating breakwater. J. Coast. Res. 73 (10073), 410–414.
Huntley, D.A., 1977. LE MÉHAUTÉ, B. 1976. An introduction to hydrodynamics and water waves. Springer-Verlag, New York, viii+ 323 p. 24.80.
Hur, Dong-Soo, Mizutani, Norimi, 2003. Numerical estimation of the wave forces acting on a three-dimensional body on submerged breakwater. Coast. Eng. 47 (3), 329–345.
Journée, J.M.J., Massie, W.W., 2001. Offshore Hydromechanics. Delft University of Technology.
Koftis, T.H., Prinos, P., Koutandos, E., 2006. 2D-V hydrodynamics of wave–floating breakwater interaction. J. Hydraul. Res. 44 (4), 451–469.
Kolahdoozan, Morteza, Bali, Meysam, Rezaee, Milad, Moeini, Mohammad Hadi, 2017. Wave-transmission prediction of π-type floating breakwaters in intermediate waters. J. Coast. Res. 33 (6), 1460–1466.
Koutandos, E., Prinos, P., Gironella, X., 2005. Floating breakwaters under regular and irregular wave forcing: reflection and transmission characteristics. J. Hydraul. Res. 43 (2), 174–188.
Macagno, E.O., 1954. Houle dans un canal présentant un passage en charge. Houille Blanche (1), 10–37.
Michael, I., 1991. Measurement of regular wave reflection. J. Waterw. Port Coast. Ocean Eng. 117 (6), 553–569.
Neelamani, S., Rajendran, R., 2002. Wave interaction with T-type breakwaters. Ocean Eng. 29 (5), 561–589.
Newman, J.N., 1977. The motion of an ideal fluid. In: Marine Hydrodynamics. pp. 102–158.
Peña, E., Ferreras, J., Sanchez-Tembleque, F., 2011. Experimental study on wave transmission coefficient, mooring lines and module connector forces with different designs of floating breakwaters. Ocean Eng. 38 (10), 1150–1160.
Rahman, Md Ataur, Mizutani, Norimi, Kawasaki, Koji, 2006. Numerical modeling of dynamic responses and mooring forces of submerged floating breakwater. Coast. Eng. 53 (10), 799–815.
Ruol, P., Martinelli, L., Pezzutto, P., 2013. Formula to predict transmission for π-type floating breakwaters. J. Waterw. Port Coast. Ocean Eng. 139 (1), 1–8.
Sadeghi, K., 2008. Significant guidance for design and construction of marine and offshore structures. GAU J. Soc. Appl. Sci. 4 (7), 65–92.
Van Rijn, L.C., 2011. Coastal erosion and control. Ocean Coast. Manag. 54 (12), 867–887.
Vugts, Jan H., 1968. The hydrodynamic coefficients for swaying, heaving and rolling cylinders in a free surface. Int. Shipbuild. Prog. 15 (167), 251–276.
Wenyang, D., Shupeng, X., Qianlong, X., Cengiz, E.R., Shan, M., 2017. Performance of an F-type floating breakwater: A numerical and experimental study. Proc. Inst. Mech. Eng. M 231 (2), 583–599.
Wiegel, R.L., 1960. Transmission of waves past a rigid vertical thin barrier. J. Waterways Harbors Division 86 (1), 1–12.
Yang, Z., 2015. Numerical and Experimental Investigation of the Performance of the Rectangular Floating Breakwater with Horizontally Extended Baseplates in Chinese. Harbin Engineering University, Harbin.
Yoshimi, G., Yasumasa, S., 1976. Estimation of incident and reflected waves in random wave experiments. In: Coastal Engineering. pp. 828–845.
Zhan, Jie-min, Chen, Xue-bin, Gong, Ye-jun, Hu, Wen-qing, 2017. Numerical investigation of the interaction between an inverse T-type fixed/floating breakwater and regular/irregular waves. Ocean Eng. 137, 110–119.
Zhang, S., Duan, W.Y., 2018. A new L type floating breakwater derived from vortex dissipation simulation. Ocean Eng. 164, 455–464.
Zheng, Y.H., You, Y.G., Shen, Y.M., 2004. On the radiation and diffraction of water waves by a rectangular buoy. Ocean Eng. 31 (8–9), 1063–1082.